Heliyon 10 (2024) e29553

Contents lists available at ScienceDirect

Heliyon

journal homepage: www.cell.com/heliyon

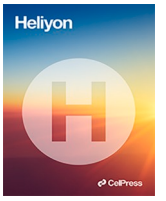

Research article

Phase formation and dielectric properties of $MgFe_2O_4$ nanoparticles synthesized by hydrothermal technique

Muhammad Tahir [a,**], Muhammad Imran [b], Zaheer H Shah [a], Muhammad Bilal Riaz [c,d,**], Saira Riaz [e], Shahzad Naseem [e]

[a] Department of Physics, University of Management and Technology, Lahore, Pakistan
[b] Department of Physics, Division of Science and Technology, University of Education, Lahore Pakistan
[c] IT4Innovations, VSB – Technical University of Ostrava, Ostrava, Czech Republic
[d] Department of Computer Science and Mathematics, Lebanese American University, Byblos, Lebanon
[e] Centre of Excellence in Solid State Physics, University of the Punjab, Lahore-54590, Pakistan

ARTICLE INFO

Keywords:
Hydrothermal
Magnetic properties
Ferromagnetic
Nanoparticles
$MgFe_2O_4$

ABSTRACT

In the recent development of energy storage devices, the scientific study has demonstrated a significant interest in the applications of the magnesium iron oxide ($MgFe_2O_4$) nanoparticles. In this work, we present synthesized novel $MgFe_2O_4$ nanoparticles at different molarities (0.1–0.5 M), via hydrothermal technique. An X-ray Diffractometer was used to study the phase analysis of the prepared samples at different molarities. A pure cubic phase of the $MgFe_2O_4$ is observed at molar concentrations of 0.3 M and 0.4 M. However, the mixed phases consisting of ($MgFe_2O_4$ + γ-Fe_2O_3) were also observed at 0.1 M, 0.2 M, and 0.5 M. The pure cubic $MgFe_2O_4$ nanoparticles depict the large value of crystallite size, 19.5 nm, and the lowest dislocation density and strain. The vibrating Sample Magnetometer shows the ferromagnetic nature of the pure $MgFe_2O_4$ with a high saturation magnetization. The value of saturation magnetization surged from 36.88 emu/g to 55.2 emu/g at 0.4 M concentration. The dielectric response of the materials as a function of applied frequency was studied thoroughly by using an Impedance Analyzer. The highest value of dielectric constant and low tangent loss was also reported at 0.4 M. Cole-Cole plots are the affirmation of the contribution of both grains and grain boundaries in the charge mechanism. These distinctive features make the synthesized material an excellent choice for future spintronics and energy storage devices.

1. Introduction

There has been a resurgence of interest in the dielectric and magnetic properties of spinel MFe_2O_4 ferrites over the past few decades. Use in optical devices, microwave electronics, tele-communication, magnetic data storage devices biomedical engineering, inductors, and power supplies are just some of the possible fields where these properties could be put to use [1–5].

$MgFe_2O_4$, in particular, has a structure of the spinel-type that is partly inverse cubic, possesses strong room-temperature chemical

** Corresponding author at: IT4Innovations, VSB – Technical University of Ostrava, 17. listopadu 2172/15, 708 00 Ostrava-Poruba, Czech Republic.
** Corresponding author.
E-mail address: muhammad.bilal.riaz@vsb.cz (M. Bilal Riaz).

https://doi.org/10.1016/j.heliyon.2024.e29553
Received 28 October 2023; Received in revised form 9 April 2024; Accepted 10 April 2024
Available online 12 April 2024

stability, and belongs to a member of the spatial Fd3m group with ã8.388 value of lattice constant [6,7]. $(Mg^{2+}_{1-\lambda}\ Fe^{3+}_{\lambda})_A\ (Mg^{2+}_{\lambda}\ Fe^{3+}_{2-\lambda})_B O_4$ is a common formula for describing cationic distribution between (A) and (B) sites i.e. tetrahedral (A) and octahedral (B) sites of such a material, that correlates with relative abundance of magnesium ions (Mg^{2+}) and iron ions (Fe^{3+}) in the (A) and (B) sites [8,9]. The parameter λ denotes the extent of cation inversion within the structural arrangement. When $\lambda = 0$, a normal spinel is produced. This indicates that (A) and (B) positions are fully occupied by Mg^{2+} and Fe^{3+} ions, respectively. On the other hand, when $\lambda = 1$, the spinel exhibits an inverted crystal structure, with Mg^{2+} ions exclusively in the (B) site and both the (A) and (B) positions contain an equal number of Fe^{3+} ions. When $0<\lambda < 1$, however, Mg^{2+} and Fe^{3+} ions coexist in (A) and (B) sites, creating a spinel structure that is partially inverted [10]. The application of heat treatments to the sample has a considerable impact on the cation distribution between (A) and (B) sites. This is primarily because Mg^{2+} ions have a high degree of diffusibility between the two sites. The ferrite's structural, magnetic, and dielectric properties may be directly affected by this phenomenon [11].

In relation to magnetic characteristics, $MgFe_2O_4$ ferrite possesses a comparatively lower T_c (curie temperature) of around ~713.15 K, unlike other ferrites like $NiFe_2O_4$, $CuFe_2O_4$, $BaFe_2O_4$, and Fe_3O_4 [12]. The material under consideration is characterized by its soft ferromagnetic properties, exhibiting a low coercivity and a moderate saturation magnetization [12,13]. Particle size, shape, and porosity all play crucial roles in determining the magnetic properties, which are themselves greatly impacted by the procedure used for sample preparation [14]. Finally, from an electrical perspective, $MgFe_2O_4$ is classified as an n-type semiconductor [15]. It is frequently characterized by its high resistivity, low dielectric loss [16,17]. The spinel ferrites have been acknowledged for their better characteristics compared to additional high-frequency magnetic materials, as a result of reduced dielectric losses and strong electrical resistivity [18–20]. The academic literature contains a wide variety of articles that examine the structural and magnetic analysis with dielectric properties of $MgFe_2O_4$ ferrites that have been doped with a wide range of ions. Magnetic and dielectric analysis of pure $MgFe_2O_4$ ferrites have only been analyzed by a small number of studies so far. The ferrites are characterized by their chemical configuration, cationic distribution, and crystallite size [21–23], as well as the manufacturing process, heat treatment, and sintering conditions, all have an impact on these characteristics. Therefore, this fact paves the way for a new and dynamic area of study.

The production method that is used will determine the physical and chemical characteristics of the synthesized particles that are produced. Therefore, it's crucial to carefully evaluate the right production method in order to achieve the desired final qualities. The usual method for producing magnesium ferrite involves combinations of oxides or carbonates in the solid state route that undergo reactions at high temperatures, often at or above 1100 °C [24]. Nevertheless, the process of high temperature synthesis is not without its downsides, including the uneven distribution of particle sizes and shapes, experiencing separation of phases, considerable energy expenditure and reactant loss.

Various production techniques have been employed to address these above said limitations, including chemical co-precipitation [25,26], sol gel route [27], self-combustion process [28], sol-gel auto-combustion route [29], microwave combustion process [30], and hydrothermal approach [31–33]. Among the several technologies available, hydrothermal synthesis stands out as a particularly promising approach. The practical application of this method has been demonstrated in the creation of several nanoparticles [34]. Hydrothermal synthesis is regarded as an environmentally sustainable method of synthesis, offering several advantages over traditional production methods. There are many benefits to using single step methods, such as increased efficiency, decreased energy consumption, accelerated reaction times, and decreased residence time [35,36]. Particle size distribution, chemical configuration, single step methods, energy consumption, reaction and residence times are also all positively affected.

Numerous researchers have documented the synthesis of magnesium iron oxide nanoparticles, as well as their characterization and the different applications they have found for them. Using a hydrothermal process, Wang et al. [37] produced BaM using mineralizers such as KOH and NaOH. On the other hand, BaM exhibited a slightly higher saturation magnetization value and a decreased coercivity value. Chen et al. [38] reported the presence of hexagonal flake in a barium ferrite $BaFe_{12}O_{19}$@PVDF composite that was synthesized through hydrothermal processing. Improvements in impedance matching and wave absorption performance were found to be proportional to the mass ratio of $BaFe_{12}O_{19}$ to PVDF, and they were most noticeable when PVDF was used as the composites' shell. The ferrites with $Ni_xMg_{1-x}Fe_2O_4$ substituents were created by Jabeen et al. [39] via hydrothermal preparation. Surface aggregation and irregular distribution of particles were shown using scanning electron microscopy. Net magnetic moment increased from 1.52 to 1.98 B and saturation magnetization value increased from 43.01 to 47.78 emu/g when the coercive field decreased. The $MgFe_{2-x}Ce_xO_4$ (x = 0.0–0.10) nanoparticles investigated by Kumar et al. [40] were synthesized using the microwave hydrothermal technique. The magnetization values of $MgFe_{2-x}Ce_xO_4$ shown low ferromagnetic behavior, ranging from 8.83 emu/g to 18.91 emu/g. The dielectric loss (tanδ) and dielectric constant (ε′) values exhibited dispersive behavior at higher frequencies and reduced with increasing frequency as a result of space-charge polarization. Using a hydrothermal technique at 80 °C, the researcher Thenila et al. [41] synthesized $MgFe_2O_4$ nanoparticles. Morphological imaging in this investigation revealed that the particles have a spherical spinel form.

The recent research is driven by a desire to understand energy storage and conduction phenomena as a function of molar concentration. Our aim is to suggest such a useful material recipe that has ultimate applications for energy storage systems. $MgFe_2O_4$ nanoparticles were synthesized by using a hydrothermal technique for first time with the variation of molar concentration (0.1M − 0.5 M). Afterwards, phase purification, magnetic and dielectric properties were studied thoroughly via different techniques for device application.

2. Experimental details

2.1. Materials

Reagent chemicals employed in this study, namely Iron Nitrate nanohydrate ($Fe(NO_3)_3.9H_2O$; 99.99 %) and Magnesium Nitrate

hexahydrate ($Mg(NO_3)_2.6H_2O$; 99.99 %), obtained from Sigma-Aldrich and were put to use without being filtered in any way. Deionized water (DI water) is employed as the solvent in the synthesis process.

2.2. Synthesis of magnesium iron oxide nanoparticles

The hydrothermal method was employed to produce nanoparticles of magnesium iron oxide. This involved the use of magnesium nitrate hexahydrate ($Mg(NO_3)_2{\cdot}6H_2O$) and iron nitrate nonahydrate ($Fe(NO_3)_3.9H_2O$) as the precursors for magnesium and iron, respectively. It has been investigated how changing the reaction parameters, such as temperature and time, affects the resulting nanoparticles. In the standard preparation procedure, magnetic stirring of 100 ml of DI water allows for the dissolution of 0.02 g Mg $(NO_3)_2{\cdot}6H_2O$ and 0.04g $Fe(NO_3)_3.9H_2O$ separately. After that, these two solutions were combined, and the final mixture rapidly stirring at room temperature, till a white uniform suspension was produced. This process was repeated until the desired consistency was reached. Eventually, the acquired suspension was placed in an autoclave made of stainless steel and Teflon, after which it was sealed and subjected to hydrothermal treatment at a constant reaction temperature in the range of 180 °C for 6 h. The acquired mixtures were permitted to cool down at RT (room temperature) before being separated in a centrifuge; a wash was carried out many times with distilled water in order to eliminate the residual contaminants, which was then followed by a wash with ethanol, which was utilized for the purpose of minimizing the agglomeration. Subsequently, the samples were exposed to a heat treatment process placed in an oven at a specific temperature of 60 °C for a duration of 2 h for the purpose of drying. The steps involved in the synthesis are laid forth in Fig. 1. After being allowed to dry, the material that had not been exposed to any moisture was then pounded into a powder using a mortar and a pestle, and then material was molded into pellets by using a hydraulic press at the pressure of 40 kg/cm^{-2}.

2.3. Characterizations

For the purpose of conducting phase analysis on magnesium iron oxide nanoparticles, an X-ray Diffractometer was operated in the range of $2\theta^\circ = 20–80^\circ$, using a step size of 0.02°. Copper was employed as the target, and the wavelength used was 1.5406 Å. The diffractometer was operated at 35 kV as accelerating potential and 25 mA as tube current. For the purpose of analyzing the magnetic properties, Lakeshore's 7407 Vibrating Sample Magnetometer (VSM) was utilized. In order to investigate the dielectric and complex impedance analysis of the material were investigated within the frequency range of $\log f = 1.3–7.4$, which corresponds to $f =$ 20Hz–20MHz, a 6500B Precision Impedance Analyzer was operated.

3. Results and discussion

3.1. XRD analysis

Fig. 2 (a) depicts the X-ray diffraction (XRD) patterns of magnesium iron oxide nanoparticles at different molar concentrations from 0.1 M to 0.5 M that were synthesized by the hydrothermal method. As shown in Fig. 2(a) magnesium iron oxide nanoparticles with 0.1

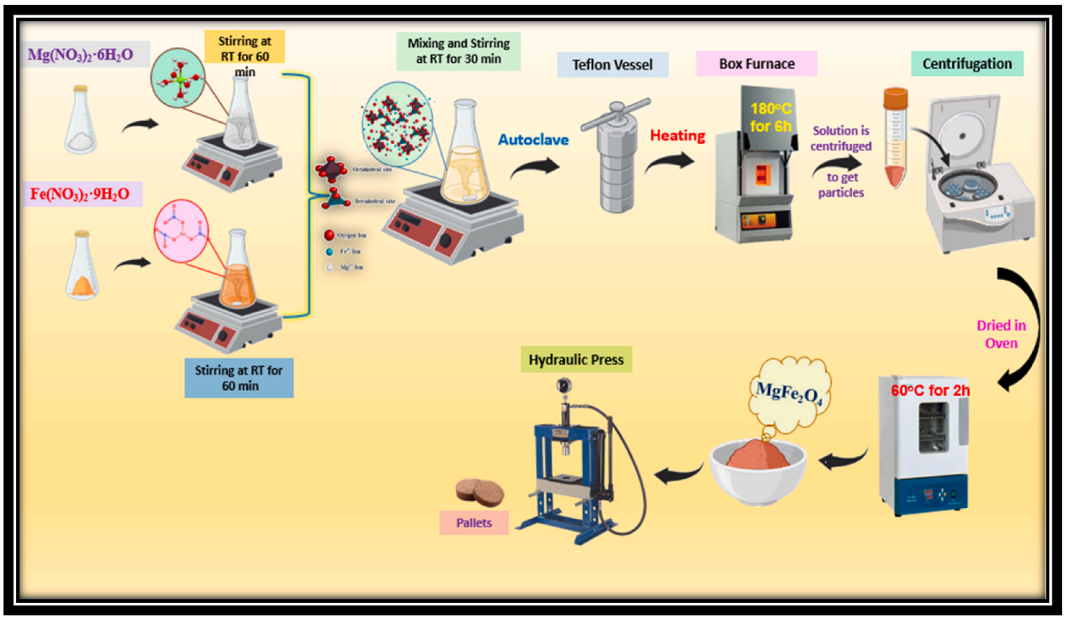

Fig. 1. Schematic diagram of synthesis process.

M–0.5 M molar concentration exhibit mixed ($MgFe_2O_4$ + ɣ-Fe_2O_3) phases. The process of structural rearrangement resulted in the formation of mixed phases, one of which was a form of ɣ-Fe_2O_3 [Fig. 2(0.1 and 0.2 M)]. The establishment of heterojunction between various phases, which can effectively segregate the spatial charges [42], is thought to be the cause of the appearance of mixed phases. Diffraction peaks for the cubic $MgFe_2O_4$ and ɣ-Fe_2O_3 phases were in excellent match with the JCPDS' card numbers 01-071-1232 and 00-039-1346. These corresponding 2θ values 35.5, 36.5, 37.1, 43.2, 53.4, 57.1, 74.2 are indexed as (311), (222), (440), (422), (511), (533) planes for pure phase while for ɣ-Fe_2O_3 the 2θ values 26.1 and 32.2 are indexed as (211) and (211) planes. Phase transformation from mixed ($MgFe_2O_4$ + ɣ-Fe_2O_3) to pure cubic phase $MgFe_2O_4$ with the molar concentration of 0.3 M and 0.4 M was evidenced by the appearance of (311), (400), (422) and (533) planes. The aforementioned change is characterized by a restructuring process, specifically the transition from mixed phases to a pure cubic phase. Fig. 2 demonstrates that at 0.3 M and 0.4 M, magnesium iron oxide nanoparticles strengthen as seen by an increase in peak intensity. The production of very pure magnesium iron oxide nanoparticles necessitates the careful tuning of several parameters. These factors include the fluctuation of valence states in Mg^{2+} and Fe^{3+} ions, as well as the maintenance of a low evaporation temperature for $MgFe_2O_4$ nanoparticles to prevent the sudden volatilization of magnesium [43]. The evaporation of Mg during the initial phases of synthesis not only results in the formation of a phase that isn't stoichiometric, nonetheless, also leads to the generation of oxygen-free spaces, hence enhancing the conduction mechanism of magnesium ferrite ($MgFe_2O_4$) nanoparticles [44]. In addition, an ionic radius of Mg^{2+} (0.085 nm) is substantially larger as compared to Fe^{3+} (0.64 nm), which is significantly smaller. Therefore, an excessive amount of Fe^{3+} causes the creation of unoccupied cationic sites, which results in $MgFe_2O_4$ spinel having a lower unit cell volume and becoming cation deficient. However, the spinel unit cell develops oxygen empty sites when it is doped with an excess of magnesium oxide (MgO), which causes the cell to expand, thereby becoming anion deficient [45]. A change from a purely phase-shifted to a state of mixed phase was once again observed when the molar concentration reached 0.5 M. This transition can be attributed to a restructuring process, as illustrated in Fig. 2(a)(0.5 M).

Rietveld's refinement was carried out for further confirmation of the phase development as depicted in Fig. 2(b–f). The goodness of fit (χ2) was confirmed by R factors. These factors are tools to identify how pure the synthesized materials were. The goodness of fit is estimated by the relation of $\chi 2 = Rwp{:}Rexp$. As the value of χ2 for all molar concentrations is closer to 1, it means that the material has a pure phase. These R factor values are enlisted in Table 1.

Using Equations (1)–(3) [46], we found the crystallite size, dislocation density, and strain. These then shown in Fig. 3.

$$t = \frac{0.9\,\lambda}{\beta\,cos\,\theta} \tag{1}$$

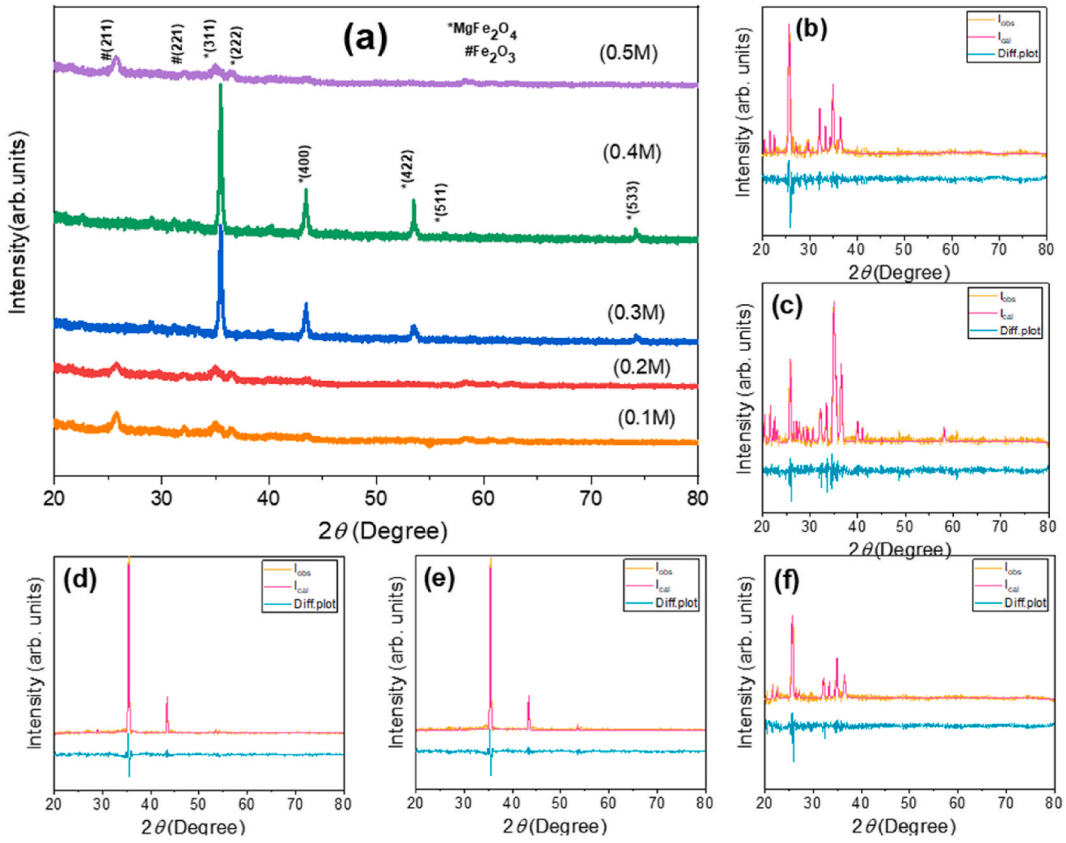

Fig. 2. (a) XRD patterns of $MgFe_2O_4$ at different molarities, (b–f) Rietveld's refinement of MFO at different molarities.

$$\delta = \frac{1}{t^2} \tag{2}$$

$$\text{Strain} = \varepsilon = \frac{\beta}{4\ tan\ \theta} \tag{3}$$

Where,

t indicates crystallite size, β depicts full width at half-maximum (FWHM)

k is the constant equals 0.94

λ represents the wavelength radiation (0.15406 nm) of Cu Kα

θ is the Bragg's angle.

Presence of different chemical or phase shifts can be observed by variations in crystallite size, as depicted in Fig. 3, in response to changes in molar concentrations. When an increase from 0.1 M to 0.3 M in molar concentration, the first chemical/phase shift became apparent. As a result of this chemical change, a change in crystal phase was noticed, from a mixed ($MgFe_2O_4$ + ɣ-Fe_2O_3) phase to a pure $MgFe_2O_4$ cubic phase. Fig. 3(a) demonstrates that at 0.3 M and 0.4 M, a steady response of increasing crystallite size was found. The observed increase in crystallite size suggests an enhancement in phase strengthening and stability, which can be attributed to a reduction in strain, as depicted in Fig. 3. At a molar concentration of 0.5 M, a second chemical or phase shift was observed. The emergence of the unstable ɣ-Fe_2O_3 phase was evidenced by a reduction in crystallite size at 0.5 M. This chemical shift resulted in the development of mixed phases ($MgFe_2O_4$ + ɣ-Fe_2O_3) once again. It's possible that two structurally competing phases emerged as a result of the provided conditions, which led to this decreasing response. Nanoparticle development is accompanied by the involvement of surface ions, interface energy, and strain energy [47,48] that can also influence the formation of nanoparticles. Moreover, particle sizes and shapes are also affected by the available energy during synthesis, which varies depending on the conditions [49]. The trend described for crystallite size variation was also observed for the change in dislocation density and strain proposed in nanoparticles [Fig. 3(b) and c)].

3.2. SEM analysis

A representation of the surface morphology of magnesium iron oxide nanoparticles can be found in Fig. 4. High molar concentrations of 0.1–0.2 M were found to result in the formation of agglomerated grains that were hard [Fig. 4(a and b)]. [Fig. 4(c–e)] shows that a relatively increased level of molarity concentration (0.3–0.5 M) led to a reduction in grain size, with less or no agglomeration and a spherical shape. The favorable synthesis circumstances have resulted in the observation of a grain with a spherical shape and defined boundaries throughout the material. As part of the chemical synthesis process, the selection of precursors, concentrations, solvents, and the methodology that is utilized are all extremely important for the nucleation of crystallites and the formation of grains [50]. When the molar concentration was increased, the grain size was seen to be large, and it exhibited a hard agglomeration. It can be concluded that the molar concentration not only had an effect on or reduced the growth of agglomerated grains, but it also assisted in the regulation of the size and shape of the nanostructures.

3.3. Magnetization analysis

In order to examine the magnetic analyses of nanoparticles of magnesium iron oxide, a vibrating sample magnetometer was utilized. Fig. 5 displays the M − H loop curves of magnesium iron oxide nanoparticles that were produced using the hydrothermal technique, with molar concentrations ranging from 0.1 M to 0.5 M. The behavior of all samples was described as being soft ferromagnetic. Fig. 6 illustrates the relationship between molar concentrations ranging from 0.1M to 0.5 M, and the corresponding values of saturation magnetization and coercivity. Chemical shift explained in light of XRD results [Fig. 2] led to a reduction in M_s (saturation magnetization) value and coercivity at a molar concentration of 0.2 M. Actually, the magnetic properties of the material are attributed as a macroscopic property so, the reduction in the saturation magnetization is may be due to the interface area, grain shape, grain size and interfacial action because these all have an effect to the magnetization. As interfacial area increase magnetic properties can be affected due to large grain [51]. A large grain can possess multiple magnetic domains and magnetization caused by these domain walls, requires less energy. Which is favorable for movement of walls to magnetize and demagnetize the material easily [52]. Nevertheless, a rise in the saturation magnetization of the cubic $MgFe_2O_4$ phase was observed when the molar concentration increased to 0.4 M, as depicted in Fig. 2(c and d). The observed rise in M_s can be ascribed to the stability of the cubic $MgFe_2O_4$ phase, as previously explained

Table 1
Rietveld's refinement data for the composite samples $MgFe_2O_4$.

Molarity (M)	0.1	0.2	0.3	0.4	0.5
R_{exp}	5.68	38.30	5.58	4.54	11.91
R_p	6.37	13.52	10.19	10.24	14.62
R_{wp}	7.05	17.79	13.35	13.18	17.79
$D_{Statistics}$	0.03	0.06	0.03	0.03	0.05
X^2	1.24	0.46	2.38	2.90	1.49

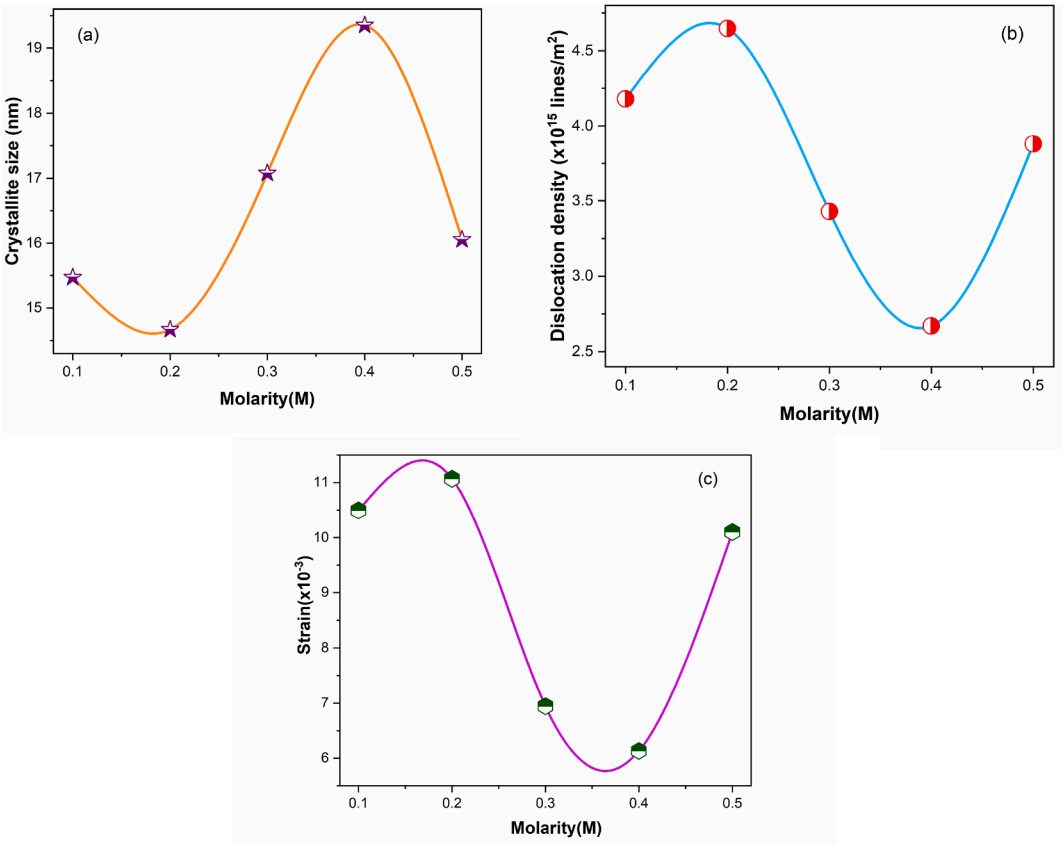

Fig. 3. Variation in (a) Crystallite size (b) dislocation density and (c) strain of magnesium iron oxide nanoparticles.

[Fig. 2(a)]. Figs. 5–6 display the soft ferromagnetic results of $MgFe_2O_4$ nanoparticles at molar concentrations of 0.2 M and 0.3 M, which were found to be in good agreement with the aforementioned phenomenon. The chemical transition from a mixed ($MgFe_2O_4$ + ɣ-Fe_2O_3) phase to a pure cubic phase $MgFe_2O_4$ phase can be attributed to the high values of M_s and H_c (coercivity) that were seen when the molar concentration was increased to 0.4 M [Fig. 2]. A significant saturation magnetization value of around 55.2 emu/g was observed at a concentration of 0.4 M. This value of M_s is highest reported value of $MgFe_2O_4$ synthesized by the hydrothermal technique to our best knowledge [53]. This observation can be attributed to the creation of a stable and strengthened cubic $MgFe_2O_4$ phase, as depicted in Fig. 6. According to the reported literature, all of the spinel's Fe^{3+} ions are found in the octahedral (B) site, while all of the spinel's Mg^{2+} ions are found in the tetrahedral (A) site. The magnetic moments that are connected with Fe^{3+} ions are principally responsible for the magnetism that is observed throughout. In addition to this, the locations that were discussed earlier are encircled by six and four oxygen atoms, respectively. All of the Fe^{3+} ions that are situated on B-sites have spin moments that are aligned in a ferromagnetic direction. Fe^{3+} ions move from tetrahedral positions carried by Mg^{2+} ions to octahedral positions occupied by Mg^{2+} ions. The aforementioned process leads to rise in the concentration of Fe^{3+} ions within octahedral sites, thus resulting in an increase of magnetization within the sublattice of octahedral positions. This, on its own, amplifies the magnetization of the nanoparticles. The shift in cationic concentration distribution [54] may account for the discrepancy in the reported value of Ms [55]. The observation is that all of the Fe^{3+} cations are ferromagnetically parallel aligned, however, provides the system with a net magnetism that is greater than zero [56]. Therefore, due to the creation of a stable and strengthened $MgFe_2O_4$ phase, the M_s and H_c values of magnesium iron oxide nanoparticles rise from 0.3 M to 0.4 M as depicted in Fig. 6(a and b).

3.4. Impedance analysis

Impedance spectroscopy is popularly recognized as a highly effective technique for evaluating the electrical behavior of thin film surfaces, bulk materials, and interfaces.

Using Eqs. (4) and (5) [57], we calculated DC (ε) and loss tangent (tanδ).

$$\varepsilon = \frac{Cd}{A\varepsilon_o} \tag{4}$$

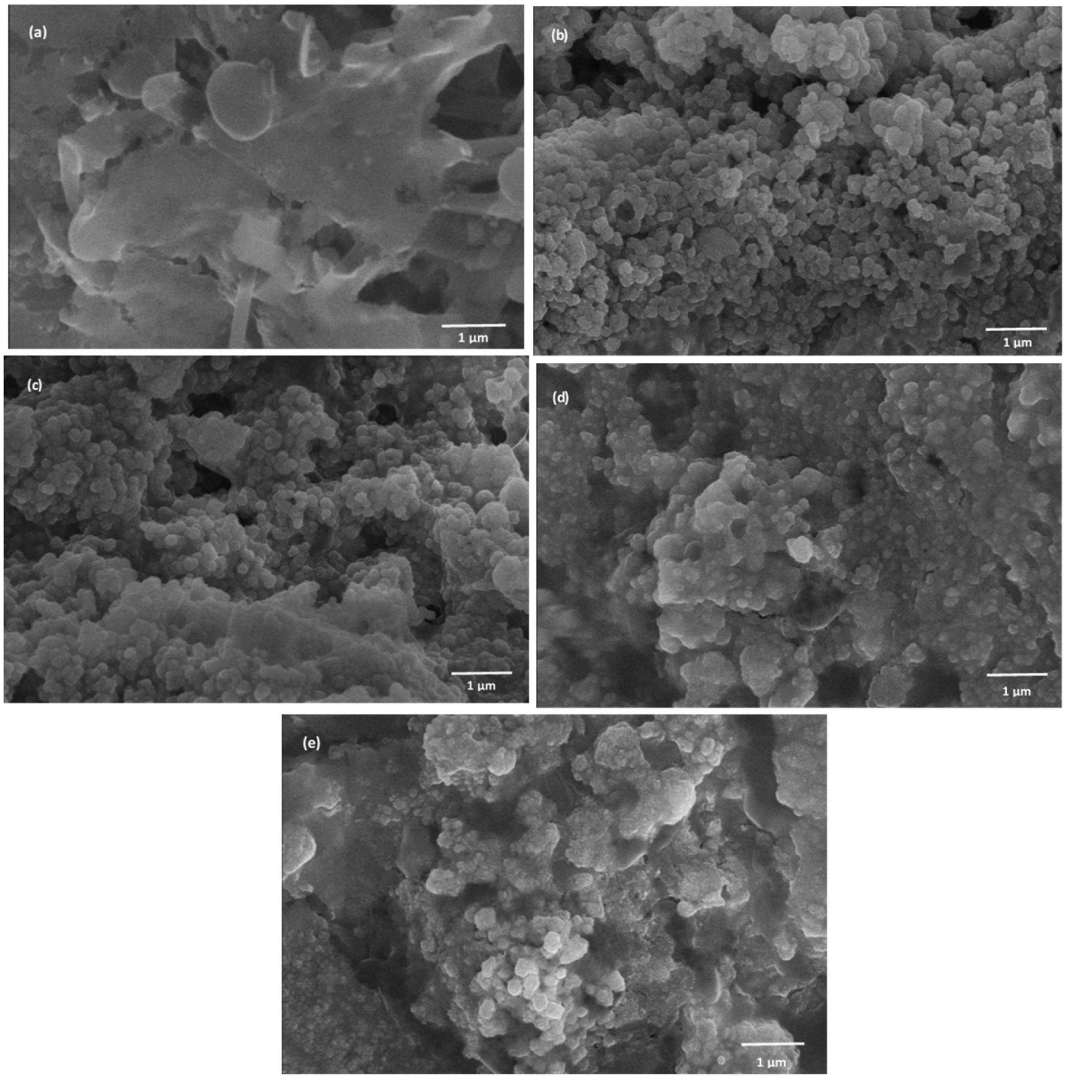

Fig. 4. SEM images of magnesium iron oxide nanoparticles with variation in molar concentration (a) 0.1 M, (b) 0.2 M, (c) 0.3 M, (d) 0.4 M and (e) 0.5 M.

$$tan\ \delta = \frac{1}{2\pi fRC} \tag{5}$$

Where, the symbol 'C' represents the quantity known as capacitance, while 'd' denotes thickness of the sample, 'A' represents cross-sectional area of sample, 'ε_{o}' represents permittivity of free space and 'R' represents resistance.

The stoichiometry of a dielectric material is a primary cause of its conductive and polarizable properties. Dipolar, space charge polarization, ionic and electronic polarization are all possible polarization events in dielectrics [58,59].

The dielectric constant (DC) and loss tangent are seen to reduce gradually in the low frequency region (Fig. 7). As the frequency increases, however, the DC (dielectric constant) is shown to be constant. Dipole relaxation, which describes the slowed motion of charge carriers within an applied electric field, is the primary cause of this dispersion in dielectric materials. In the low frequency region, electrons produce polarization due to the accumulation of the charges at grain boundaries but at higher frequencies this polarization vanishes due to the reverse direction of electron. Moreover, at higher frequencies, the contribution made by electrical polarization is significant due to the different polarization mechanisms including electron and ion displacement mechanism [60,61]. The phenomenon of polarization is accountable for the decrease in the electric field strength within a given medium. The conduction process at high frequencies involves the participation of grains, as proposed the theory by Koop and the two layered model by Maxwell-Wagner [51,62,63]. In contrast, grain boundaries are only involved at very low frequencies. These simulations suggest that the dielectric analysis/properties of magnesium iron oxide nanoparticles are due to a combination of the effects of grains that conduct electricity and grain borders that do not conduct electricity. In order to carry out the exchange interaction, electrons in poly-crystalline

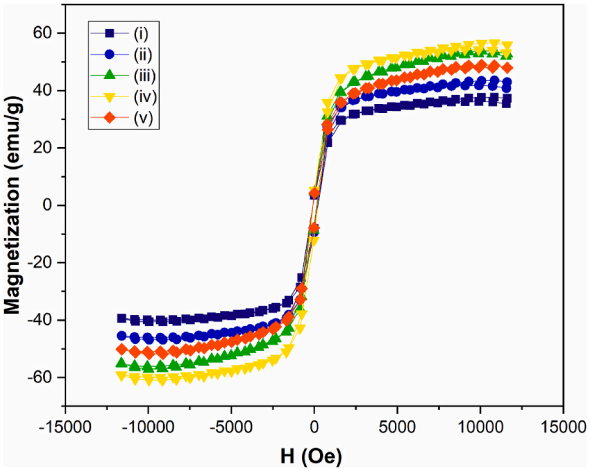

Fig. 5. M − H loops of magnesium iron oxide nanoparticles with variation in molar concentration (i) 0.1 M, (ii) 0.2 M, (iii) 0.3 M, (iv) 0.4 M and (v) 0.5 M.

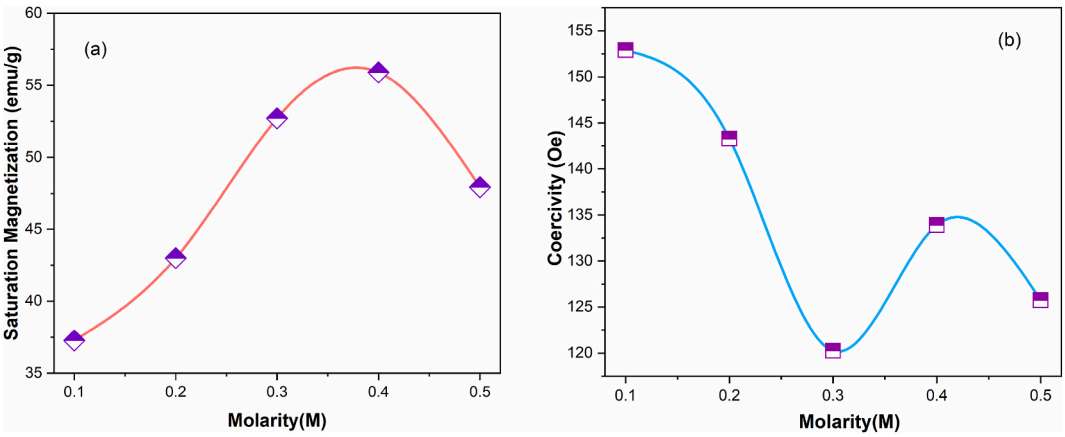

Fig. 6. Variation in (a) saturation magnetization and (b) coercivity of magnesium iron oxide nanoparticles with varying molar concentration.

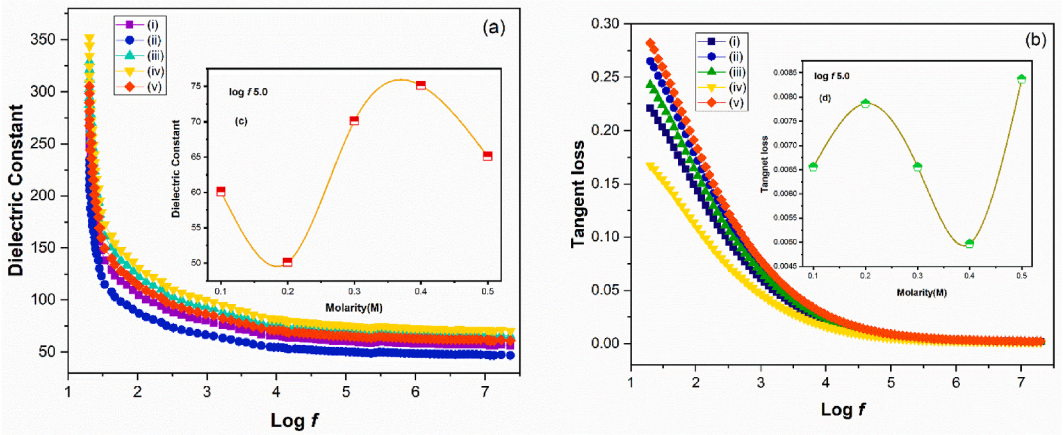

Fig. 7. Variation in (a) dielectric constant and (b) tangent loss of magnesium iron oxide nanoparticles with frequency; where (i–v) 0.1M–0.5 M molar concentration; inset (c) and (d) shows the variation with the changes in molar concentration.

materials must be able to tunnel between the grains and across the grain boundaries. The barrier that is generated by grain boundaries can, on the other hand, make the hopping of electrons more difficult, which may lead to a reduction in conduction. This process causes charge carriers to accumulate at grain boundaries, which in turn generates space charge polarization [64].

The calculation of losses in material applications is of utmost importance, and the loss tangent represents the dissipation of energy that emerges owing to the applied electric field that leads the polarization. There could be three types of losses i.e conduction loss, resonance and relaxation loss. In the measurement of frequency conduction loss plays a vital role. These conduction losses decreased at high frequencies due to reduction of joule heating [65]. The structural and the chemical composition of material, the process used to synthesize it, and the temperature all play a vital role in determining the value of the loss tangent. The dielectric loss is noticeable at low frequencies, but it is unnoticeable at high frequencies [51,66]. When the rate at which electrons transition between Mg^{2+} and Fe^{3+} ions located at tetrahedral and octahedral sites exceeds the strength of the externally applied field, there is a significant increase in losses due to the exchange interaction of electrons, which exhibits a strong response to the applied field. In addition to this, resistive grain boundaries are another factor that contributes to high loss tangent. As a result, charge carriers need a greater amount of energy to transition from the anionic state of Fe^{2+} to the cationic state of Fe^{3+} [67]. This is because the concentration of Fe^{3+} ions is higher. In contrast, at higher frequencies, losses are reduced because the electron exchange process does not adopt the frequency of the applied field. Here, though, there was no peak found for any of our samples, which further supports the idea that Fe^{2+} ions are not contributive to the response of dielectric. In addition, the distribution of cations, highly resistance samples and accordingly reduced values of DC (dielectric constant) and factor of dielectric loss rule out the chances of the occurrence of Fe^{2+} ions that would have an effect on the dielectric performance of the magnesium ferrites that were examined in this study [68].

Fig. 7(c and d) illustrates plots of the DC and the loss tangent at log *f* 5.0 as functions of the molar concentration. Magnesium iron oxide nanoparticles with a molar concentration of 0.1 M exhibited a DC (dielectric constant) of ~75 at about log *f* 5.0 [Fig. 7(c)]. The dielectric constant was found to be relatively small at a molar concentration of 0.2 M. It is possible that the low availability of Fe^{3+} ions at octahedral (B) site, which is preferably occupied by Mg^{2+} ions, was the cause of the drop in the dielectric constant that was seen in response to rise in the concentration of Mg^{2+} and Fe^{3+} ions for 0.2 M. A significantly high dielectric constant value of around ~77 was observed for $MgFe_2O_4$ at a molar concentration of 0.4 M, specifically at log *f* 5.0. Phase stability and strengthening of $MgFe_2O_4$, as mentioned in the structural results [Fig. 2], led to an increase in dielectric constant at 0.3 M and 0.4 M. Moreover, at a molar concentration of 0.5 M, the dielectric constant was found to be relatively small. The amount of time that is available for charge carriers in space to align themselves in the direction of an electric field gets shorter as the frequency gets higher. This leads in lower polarization, which in turn results in a decreased dielectric constant [69,70]. Due to the presence of both cations, Mg^{2+} and Fe^{3+}, in $MgFe_2O_4$, it is possible that this material will have a greater value of DC and a lower value of loss tangent when compared to 0.1 M, 0.2 M, and 0.5 M, respectively. The nanoparticles of $MgFe_2O_4$ are subjected to the combined influence of $Mg^{2}+$ and Fe^{3+} ions. Two examples of favorable dielectric qualities exhibited by a material are a low value of loss tangent and a high value of dielectric constant. The application possibilities of composites are affected by a variety of factors like the shape, size, and dielectric constants of constituent materials [71].

Dielectric constant (ε) and tangent loss (tanδ) were used in Eq. (6) [49–55] to determine the conductivity (σ) of magnesium iron oxide nanoparticles.

$$\sigma = 2\pi f \varepsilon \varepsilon_o \tan\delta \tag{6}$$

where frequency is represented by *f*, dielectric constant is ε, the permittivity of free space is ε_o.

Fig. 8 displays the conductivity plots of magnesium iron oxide nanoparticles versus log *f*. The concept of frequency dependent conductivity provides an explanation for the mechanisms and processes that are involved in transport through dielectrics. Both dc-like

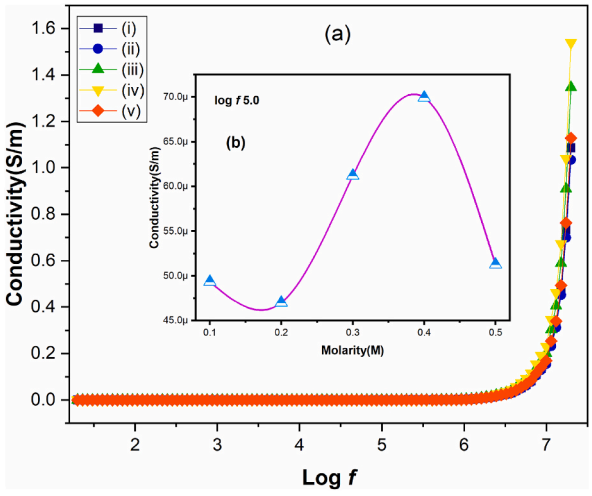

Fig. 8. Variation in conductivity with (a) frequency and (b) molar concentration of magnesium iron oxide nanoparticles for (i) 0.1 M, (ii) 0.2 M, (iii) 0.3 M, (iv) 0.4 M and (v) 0.5 M; inset depicts the variation in molar concentration.

and ac conductivities contribute to the total conductivity. Due to band conduction at low frequencies, dc-like conductivity is frequency independent. Instead, the ac conductivity is a frequency-dependent response caused by the transfer of electrons between cations with different valences. In an ideal dielectric material, there are no free charge carriers so there is no possibility of dc like conduction occurring. Tunneling allows charge carriers to be able to make transition from one bound state to another, which is the only mechanism that allows ac conduction to take place [65]. Though, in this work the dc-like conductivity that is observed arises as a result of the presence of conduction between bound states, whilst the ac conductivity that is observed arises as a result of the hopping conduction mechanism that is observed among the various localized states. Because dielectric materials have very few charge carriers available, their conductivity is a mixture of dc and ac conductivity, as stated in Eq. (7) [55]. As a result, the conductivity of dielectric materials is the same as this combination.

$$\sigma(\omega) = \sigma_{d.c} + \sigma_{a.c}(\omega) \tag{7}$$

The term "universal dielectric response" refers to the phenomenon in which the conductivity of a material varies as a function of the frequency; more specifically, the frequency causes an increase in the conductivity. The response is readily explained by the fact that at high frequencies, the hopping process between the ions of Fe^{2+} and Fe^{3+} is amplified. This enhanced hopping is the result of a rise in the mobility of charge carriers originating from a variety of different trapping centers [63]. A significant rise in conductivity was found when the log *f* reached 5.0, accompanied by an increase in molar concentration to 0.4 M, as depicted in Fig. 8(b). The decrease in conductivity as the concentration of Mg^{2+} ions increase can be explained by the greater number of Mg^{2+} cations, which hinder the conduction between $Fe^{3+} \leftrightarrow Fe^{2+}$ions because Mg^{2+} ions occupy an octahedral site [64]. Since grain borders are more active than grains, the hopping phenomena between Fe^{2+} and Fe^{3+} ions decrease in the low-frequency regime, leading to reduced conductivity values. The conductivity values rise in the high-frequency area because the grains are more energetic than the grain borders, which promotes hopping mechanism between the ions of Fe^{2+} and Fe^{3+}.

Following are some equations that were used to calculate real and imaginary impedances [71]:

$$Z* = Z' + i\,Z'' \tag{8}$$

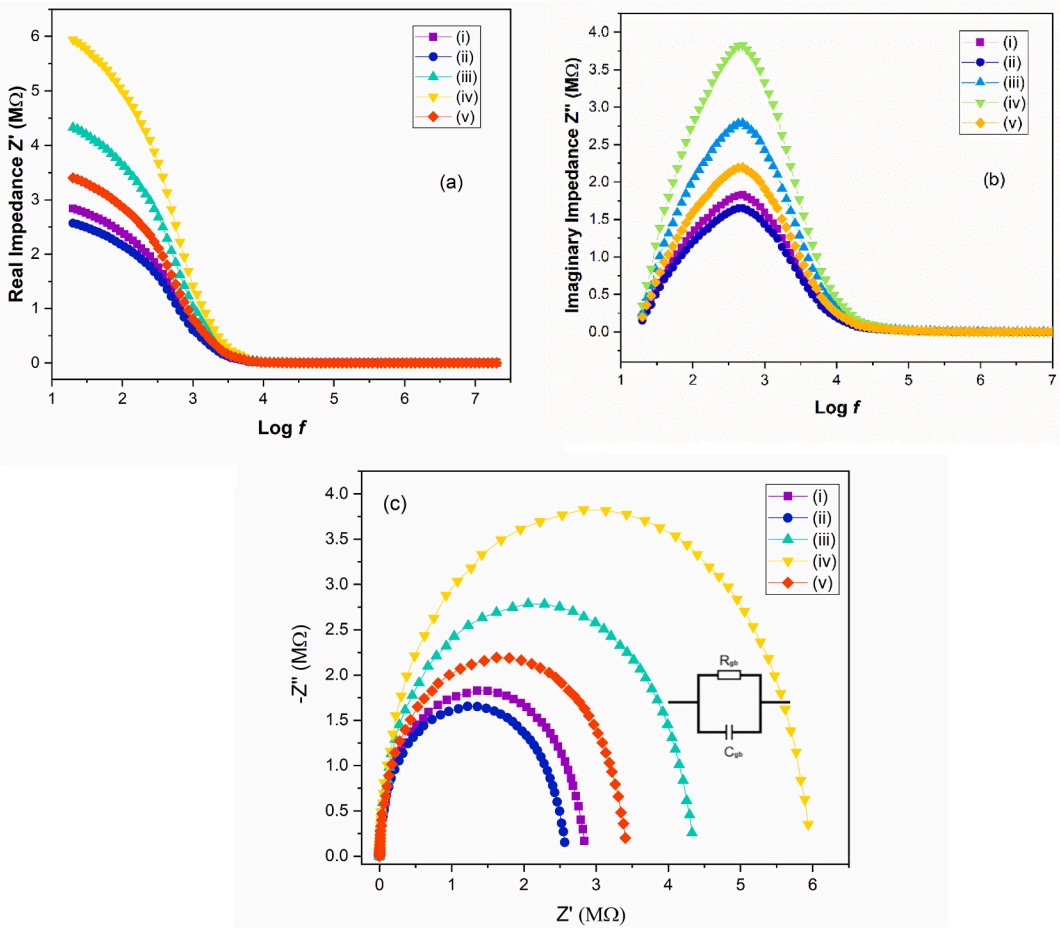

Fig. 9. (a) Real, (b) Imaginary impedance and (c) Cole-Cole plots (inset shows the equivalent circuit) of magnesium iron oxide nanoparticles for (i–v) 0.1M − 0.5 M molar concentration.

$$Z' = Z \cos \theta \tag{9}$$

$$Z'' = Z \sin \theta \tag{10}$$

The resistive and reactive components of Z* are signified by Z' and Z'' respectively. These components provide data pertaining to the conductivity and resistivity of the material. The impedance characteristics of magnesium iron oxide nanoparticles are represented in Fig. 9(a and b), illustrating both the real and imaginary components. As a result of predominate influence of space charge carrier polarization [72], researchers found that real impedance exhibited nearly constant behavior at lower frequency values ($\log f > 4.0$). The discovery facilitated by this fact that the real impedance exhibited a reduction as the frequency increased. As can be seen in Fig. 9 (a)–as the frequency increases ($\log f > 4.0$), the actual impedance (Z) decreases due to the considerable barrier qualities of materials [68]. Therefore, as previously mentioned in the manuscript, grain boundaries that serve as obstacles to conduction have a reduced impact on resistance. The impedance exhibits a decreasing trend that transitions to a virtually constant response at the highly region of applied frequency. At higher frequency values, the relaxation time for space charge carriers is insufficient. As can be seen in Fig. 9, this merging of plots is the result of the decreased polarization caused by the increased recombination rate in response to the space charge. At long last, the value of the real impedance is shown to be independent of frequency. There was a clear correlation between the rise in molar concentration and the Z' value. Maximum values for imaginary impedance were measured, as depicted in Fig. 9(b). The Z'' plot reveals 3 significant features, which are as follows: (i) there is a shift in the peak's position to higher frequencies; (ii) a reduction in peak's height in response to an increase in molar concentration; and (iii) a reduction in peak breadth in response to an increase in molar concentration. The relaxation process in magnesium iron oxide nanoparticles is characterized by a relative widening as well as a shift in the position of the peak. At higher molar concentrations, the relaxation process is caused by immobile electrons in addition to any defects that may be present. Because of the bulk resistance, one can detect a shift in the peak location towards higher frequencies as the molar concentration increases. whereas an increase in molar concentration is responsible for a lower peak height as a result of accumulating space charge carriers at low frequencies [73,74].

Fig. 9(c) depicts the study of Cole-Cole plots (Nyquist plots) to differentiate between the grains and grain boundaries' contribution to the conduction mechanism. Depending on the electrical properties of the materials being plotted, the Cole-Cole plots produce either one, two, or three semicircles as a result. Resistance of grain boundaries is connected with the development of a semicircle at lower frequencies. The development of distinct semicircles is dependent on the frequency, and the contribution/involvement of grains, grain boundaries, and the interface between grains are all represented by these semicircles [75]. According to Fig. 9(c), there was one semicircle that was observed during the course of this investigation that suggested significant resistance of grain boundary. The values of grain boundary resistance and capacitance extracted from EC lab are given in Table 2. Keeping an eye on all the features discussed above the material can be employed to data and energy storage devices.

4. Conclusions

In this paper, the magnesium iron oxide was convincingly studied with the variation in the molarities. The hydrothermal technique was employed to achieve the synthesis of nanoparticles of $MgFe_2O_4$. An X-ray diffractometer was used to investigate the structural properties of the samples. Mixed phases $MgFe_2O_4 + Fe_2O_3$ were observed at molar concentrations of 0.1 M, 0.2 M, and 0.5 M, while Sharp intensities at 0.3 and 0.4 M confirmed the presence of a pure phase of cubic spinel $MgFe_2O_4$ with the space group Fd-3m. At different molarities, phase transitions result in tunable crystallite size, dislocation density, and strain energy. As a function of molarity, maximum magnetization (M_s) was increased first from 36.88 emu/g to 55.23 emu/g and then the value of magnetization dropped to 47.9 emu/g. The highest value of M_s is observed at 0.4 M concentration. The frequency dependent dielectric properties were studied. Maxwell-Wagner theory demonstrated the frequency dispersion of these parameters. A high value of dielectric constant of ~75.5 ($\log f$ 5.0) was observed at 0.4 M concentration. The dielectric response of magnesium iron oxide nanoparticles was significantly influenced by the resistance at grain boundaries. Conclusively, these valuable feature of the novel material makes the $MgFe_2O_4$ potential candidate for the memory and data storage devices.

5. Data availability statement

All relevant data has been used in the manuscript.

CRediT authorship contribution statement

Muhammad Tahir: Writing – original draft, Data curation. **Muhammad Imran:** Resources, Investigation. **Zaheer H Shah:** Formal analysis, Conceptualization. **Muhammad Bilal Riaz:** Investigation, Validation, Supervision, Funding acquisition, Software. **Saira Riaz:** Writing – review & editing. **Shahzad Naseem:** Visualization, Supervision.

Declaration of competing interest

The authors declare that they have no known competing financial interests or personal relationships that could have appeared to influence the work reported in this paper.

Table 2
Grain boundary resistance and capacitance values extracted using EC lab software.

Sample ID	R_{gb} (MΩ)	C_{gb} (pF)
i	2.83	20.2
ii	2.56	195.0
iii	4.33	116.0
iv	5.94	83.9
v	3.4	147.0

Acknowledgement

The Author Muhammad Bilal Riaz is highly thankful to Ministry of Education, Youth and Sports of the Czech Republic for their support through the e-INFRA CZ (ID:90254).

References

[1] C. Gómez-Polo, V. Recarte, L. Cervera, J.J. Beato-López, J. López-García, J.A. Rodríguez-Velamazán, M.D. Ugarte, J.G.S. Duque, Tailoring the structural and magnetic properties of Co-Zn nanosized ferrites for hyperthermia applications, J. Magn. Magn Mater. 465 (2018) 211–219.
[2] A. Omri, E. Dhahri, B.F.O. Costa, M.A. Valente, Structural, electric and dielectric properties of Ni0. 5Zn0. 5FeCoO4 ferrite prepared by sol-gel, J. Magn. Magn Mater. 499 (2020) 166243.
[3] Y. Shen, Y. Wu, X. Li, Q. Zhao, Y. Hou, One-pot synthesis of MgFe2O4 nanospheres by solvothermal method, Mater. Lett. 96 (2013) 85–88.
[4] M. Siva Ram Prasad, K.V. Ramesh, B.R. Babu, K. Trinath, DC electrical resistivity and dielectric properties of Ni–Zn nanoferrite synthesized via autocombustion route, Indian J. Phys. 90 (2016) 417–428.
[5] Y.P. Fu, S.H. Hu, Electrical and magnetic properties of magnesium-substituted lithium ferrite, Ceram. Int. 36 (4) (2010) 1311–1317.
[6] B. Aslibeiki, G. Varvaro, D. Peddis, P. Kameli, Particle size, spin wave and surface effects on magnetic properties of MgFe2O4 nanoparticles, J. Magn. Magn Mater. 422 (2017) 7–12.
[7] Z.K. Heiba, M.B. Mohamed, Effect of magnesium deficiency on magnetic properties tuning and cation redistributions of magnesium ferrite nanoparticles, J. Mater. Sci. Mater. Electron. 30 (2019) 786–796.
[8] M.G. Naseri, M.H.M. Ara, E.B. Saion, A.H. Shaari, Superparamagnetic magnesium ferrite nanoparticles fabricated by a simple, thermal-treatment method, J. Magn. Magn Mater. 350 (2014) 141–147.
[9] F. Nakagomi, S.W. Da Silva, V.K. Garg, A.C. Oliveira, P.C. Morais, A. Franco Jr, Influence of the Mg-content on the cation distribution in cubic MgxFe3− xO4 nanoparticles, J. Solid State Chem. 182 (9) (2009) 2423–2429.
[10] N. Aliyan, S.M. Mirkazemi, S.M. Masoudpanah, S. Akbari, The effect of post-calcination on cation distributions and magnetic properties of the coprecipitated MgFe2O4 nanoparticles, Appl. Phys. A 123 (2017) 1–7.
[11] Y. Ichiyanagi, M. Kubota, S. Moritake, Y. Kanazawa, T. Yamada, T. Uehashi, Magnetic properties of Mg-ferrite nanoparticles, J. Magn. Magn Mater. 310 (2) (2007) 2378–2380.
[12] B.D. Cullity, C.D. Graham, Introduction to Magnetic Materials, 2nd ed., Willey-IEEE press, 2011, 168
[13] Y. Feng, S. Li, Y. Zheng, Z. Yi, Y. He, Y. Xu, Preparation and characterization of MgFe2O4 nanocrystallites via PVA sol-gel route, J. Alloys Compd. 699 (2017) 521–525.
[14] Y. Huang, Y. Tang, J. Wang, Q. Chen, Synthesis of MgFe2O4 nanocrystallites under mild conditions, Mater. Chem. Phys. 97 (2–3) (2006) 394–397.
[15] A.G. Abraham, A. Manikandan, E. Manikandan, S. Vadivel, S.K. Jaganathan, A. Baykal, P.S. Renganathan, Enhanced magneto-optical and photo-catalytic properties of transition metal cobalt (Co2+ ions) doped spinel MgFe2O4 ferrite nanocomposites, J. Magn. Magn Mater. 452 (2018) 380–388.
[16] V. Jeseentharani, M. George, B. Jeyaraj, A. Dayalan, K.S. Nagaraja, Synthesis of metal ferrite (MFe2O4, M= Co, Cu, Mg, Ni, Zn) nanoparticles as humidity sensor materials, J. Exp. Nanosci. 8 (3) (2013) 358–370.
[17] D.K. Mahato, S. Banerjee, Dielectric characteristics of MgFe2O4 ferrite prepared by sol-gel auto-combustion method, Mater. Today: Proc. 4 (4) (2017) 5525–5531.
[18] S.I. Hussein, A.S. Elkady, M.M. Rashad, A.G. Mostafa, R.M. Megahid, Structural and magnetic properties of magnesium ferrite nanoparticles prepared via EDTA-based sol–gel reaction, J. Magn. Magn Mater. 379 (2015) 9–15.
[19] R. Sagayaraj, S. Aravazhi, G. Chandrasekaran, Microstructure and magnetic properties of Cu0. 5Co0. 3Mo0. 2Fe2O4 ferrite nanoparticles synthesized by coprecipitation method, Appl. Phys. A 127 (7) (2021) 502.
[20] C. Choodamani, B. Rudraswamy, G.T. Chandrappa, Structural, electrical, and magnetic properties of Zn substituted magnesium ferrite, Ceram. Int. 42 (9) (2016) 10565–10571.
[21] K. Nadeem, F. Zeb, M.A. Abid, M. Mumtaz, M.A. ur Rehman, Effect of amorphous silica matrix on structural, magnetic, and dielectric properties of cobalt ferrite/silica nanocomposites, J. Non-Cryst. Solids 400 (2014) 45–50.
[22] K.C.B. Naidu, W. Madhuri, Microwave hydrothermal synthesis: structural and dielectric properties of nano MgFe2O4 ceramics, Mater. Today: Proc. 3 (10) (2016) 3810–3813.
[23] P. Heidari, S.M. Masoudpanah, Structural and magnetic properties of MgFe2O4 powders synthesized by solution combustion method: the effect of fuel type, J. Mater. Res. Technol. 9 (3) (2020) 4469–4475.
[24] A.I. Turkin, V.A. Drebushchak, Synthesis and calorimetric investigation of stoichiometric Fe-spinels: MgFe2O4, J. Cryst. Growth 265 (1–2) (2004) 165–167.
[25] Q. Chen, A.J. Rondinone, B.C. Chakoumakos, Z.J. Zhang, Synthesis of superparamagnetic MgFe2O4 nanoparticles by coprecipitation, J. Magn. Magn Mater. 194 (1–3) (1999) 1–7.
[26] C.P. Liu, M.W. Li, Z. Cui, J.R. Huang, Y.L. Tian, T. Lin, W.B. Mi, Comparative study of magnesium ferrite nanocrystallites prepared by sol–gel and coprecipitation methods, J. Mater. Sci. 42 (2007) 6133–6138.
[27] A. Pradeep, P. Priyadharsini, G. Chandrasekaran, Sol–gel route of synthesis of nanoparticles of MgFe2O4 and XRD, FTIR and VSM study, J. Magn. Magn Mater. 320 (21) (2008) 2774–2779.
[28] S.V. Bangale, D.R. Patil, S.R. Bamane, Preparation and electrical properties of nanocrystalline MgFe2O4 oxide by combustion route, Arch. Appl. Sci. Res. 3 (5) (2011) 506–513.
[29] Y. Feng, S. Li, Y. Zheng, Z. Yi, Y. He, Y. Xu, Preparation and characterization of MgFe2O4 nanocrystallites via PVA sol-gel route, J. Alloys Compd. 699 (2017) 521–525.
[30] D. Chen, Y. Zhang, C. Tu, Preparation of high saturation magnetic MgFe2O4 nanoparticles by microwave-assisted ball milling, Mater. Lett. 82 (2012) 10–12.
[31] J. Nonkumwong, S. Ananta, P. Jantaratana, S. Phumying, S. Maensiri, L. Srisombat, Phase formation, morphology and magnetic properties of MgFe2O4 nanoparticles synthesized by hydrothermal technique, J. Magn. Magn Mater. 381 (2015) 226–234.
[32] T. Sasaki, S. Ohara, T. Naka, J. Vejpravova, V. Sechovsky, M. Umetsu, S. Takami, B. Jeyadevan, T. Adschiri, Continuous synthesis of fine MgFe2O4 nanoparticles by supercritical hydrothermal reaction, J. Supercrit. Fluids 53 (1–3) (2010) 92–94.

[33] S. Verma, P.A. Joy, Y.B. Khollam, H.S. Potdar, S.B. Deshpande, Synthesis of nanosized MgFe2O4 powders by microwave hydrothermal method, Mater. Lett. 58 (6) (2004) 1092–1095.
[34] K. Byrappa, T. Adschiri, Hydrothermal technology for nanotechnology, Prog. Cryst. Growth Char. Mater. 53 (2) (2007) 117–166.
[35] K. Byrappa, M. Yoshimura, Handbook of Hydrothermal Technology, William Andrew, 2012, 2nd ed.
[36] W.L. Suchanek, R.E. Riman, Hydrothermal synthesis of advanced ceramic powders, Adv. Sci. Technol. 45 (2006) 184–193.
[37] M. Ijaz, H. Ullah, B.A. Al-Asbahi, M.U. Khan, Z. Abbas, S.U. Asif, Co-precipitation method followed by ultrafast sonochemical synthesis of aluminium doped M type BaFe11. 4-xAlxCo0. 6O19 hexaferrites for various applications, J. Magn. Magn Mater. 589 (2024) 171559.
[38] C. Chen, G. Chen, F. Chen, Z. Zhang, J. Wang, Z. Su, Z. Zhou, Y. Ma, W. Cai, R. Gao, Achieving superior electromagnetic-absorbing performances in the hexagonal flake BaFe12O19@ PVDF composites, Inorg. Chem. 63 (1) (2023) 353–368.
[39] Z. Jabeen, A. Dawood, M. Alomar, S.N. Khan, I. Ali, M. Asif, W. Abbas, M.S. Irshad, M. Ahmad, Hydrothermal synthesis of nickel substituted magnesium ferrites (NixMg1-xFe2O4) and insight into the detailed structural, magnetic and electrochemical properties, Surface. Interfac. 40 (2023) 103130.
[40] T.S. Kumar, G. Sriramulu, P. Raju, T. Ramesh, K. Praveena, S. Katlakunta, Structural, optical, magnetic and dielectric properties of Ce-doped MgFe2O4 prepared by microwave hydrothermal method, ECS Journal of Solid State Science and Technology 12 (9) (2023) 093014.
[41] K. Thenila, S. Rathinavel, R. Deepika, Synthesis and charcterization of magnesium ferrite ($MgFe_2O_4$) nanoparticles by hydrothermal method, International Research Journal of Modernization in Engineering Technology and Science 5 (4) (2023).
[42] C.M. Hussain, A.K. Mishra, Nanotechnology in Environmental Science, 2 Volumes, vol. 1, John Wiley & Sons, 2018, p. 920.
[43] J. Li, M. Zhang, B. Li, S.N. Monteiro, S. Ikhmayies, Y.E. Kalay, J.Y. Hwang, J.P. Escobedo-Diaz, A.D. Brown (Eds.), Characterization of Minerals, Metals, and Materials 2020, vol. 751, Springer Nature, 2020.
[44] L. Fu, H. Chen, K. Wang, X. Wang, Oxygen-vacancy generation in MgFe2O4 by high temperature calcination and its improved photocatalytic activity for CO2 reduction, J. Alloys Compd. 891 (2022) 161925.
[45] M.F. Zawrah, Investigation of lattice constant, sintering and properties of nano Mg–Al spinels, Materials Science and Engineering: A 382 (1–2) (2004) 362–370.
[46] B.D. Cullity, Elements of X-Ray Diffraction, Addison-Wesley, 1956, 3rd ed.). Addison-Wesley, 514.
[47] A. Selmani, D. Kovačević, K. Bohinc, Nanoparticles: from synthesis to applications and beyond, Adv. Colloid Interface Sci. 303 (2022) 102640.
[48] M. Rai, B. Zimowska, G.J. Kövics (Eds.), Phoma: Diversity, Taxonomy, Bioactivities, and Nanotechnology, Springer, 2022, p. 342, 1st ed.
[49] E.M. Egorova, A.A. Kubatiev, V.I. Schvets, Biological Effects of Metal Nanoparticles, Springer International Publishing, Cham, 2016, p. 79, 1st ed.
[50] K.J. Wu, C.M. Edmund, C. Shang, Z. Guo, Nucleation and growth in solution synthesis of nanostructures–from fundamentals to advanced applications, Prog. Mater. Sci. 123 (2022) 100821.
[51] R. Gao, X. Qin, Q. Zhang, Z. Xu, Z. Wang, C. Fu, G. Chen, X. Deng, W. Cai, Enhancement of magnetoelectric properties of (1-x) Mn0. 5Zn0. 5Fe2O4-xBa0. 85Sr0. 15Ti0. 9Hf0. 1O3 composite ceramics, J. Alloys Compd. 795 (2019) 501–512.
[52] L. Lv, J.P. Zhou, Q. Liu, G. Zhu, X.Z. Chen, X.B. Bian, P. Liu, Grain size effect on the dielectric and magnetic properties of NiFe2O4 ceramics, Phys. E Low-dimens. Syst. Nanostruct. 43 (10) (2011) 1798–1803.
[53] N. Kumari, R. Jasrotia, S. Kour, N. Neha, Y. Singh, R. Kumar, Synthesis methods and magnetic properties of magnesium ferrites: a short review, in: AIP Conference Proceedings, AIP Publishing, 2022, May (Vol. 2357, No. 1.
[54] J. Smit, H.P.J. Wijn, Ferrites, Cleaver-Hume Press, 1959, 1st ed.
[55] J. Ebenezar, Recent Trends in Materials Science and Applications, Springer, 2017, p. 396, 1st ed.
[56] A. Fernandez-Pacheco, Studies of Nanoconstrictions, Nanowires and Fe3O4 Thin Films: Electrical Conduction and Magnetic Properties. Fabrication by Focused Electron/ion Beam, 1st ed., Springer Berlin Heidelberg, 2011, 188
[57] E. Barsoukov, J.R. Macdonald, Impedance Spectroscopy Theory, Experiment, and Applications, John Wiley &Sons, 2005, p. 595, 2nd ed.
[58] M. Maglione, M.A. Subramanian, Dielectric and polarization experiments in high loss dielectrics: a word of caution, Appl. Phys. Lett. 93 (3) (2008).
[59] S.M.H. Shah, A. Akbar, S. Riaz, S. Atiq, S. Naseem, Magnetic, structural, and dielectric properties of Bi1-xKxFeO3 thin films using sol-gel, IEEE Trans. Magn. 50 (8) (Aug. 2014) 1–4, https://doi.org/10.1109/TMAG.2014.2310691. Art no. 2201004.
[60] R. Gao, Z. Wang, G. Chen, X. Deng, W. Cai, C. Fu, Influence of core size on the multiferroic properties of CoFe2O4@ BaTiO3 core shell structured composites, Ceram. Int. 44 (2018) S84–S87.
[61] R. Xu, S. Zhang, F. Wang, Q. Zhang, Z. Li, Z. Wang, R. Gao, W. Cai, C. Fu, The study of microstructure, dielectric and multiferroic properties of (1−x) Co 0.8 Cu 0.2 Fe 2 O 4-x Ba 0.6 Sr 0.4 TiO 3 composites, J. Electron. Mater. 48 (2019) 386–400.
[62] M. Imran, A. Akbar, S. Riaz, S. Atiq, S. Naseem, Electronic and structural properties of phase-pure magnetite thin films: effect of preferred orientation, J. Electron. Mater. 47 (11) (2018) 6613–6624.
[63] H. Wu, R. Xu, C. Zhou, S. Xing, Z. Zeng, H. Ao, W. Li, X. Qin, R. Gao, Effect of core size on the magnetoelectric properties of Cu0. 8Co0. 2Fe2O4@ Ba0. 8Sr0. 2TiO3 ceramics, J. Phys. Chem. Solid. 160 (2022) 110314.
[64] F. Hcini, S. Hcini, M.A. Wederni, B. Alzahrani, H. Al Robei, K. Khirouni, S. Zemni, M.L. Bouazizi, Structural, optical, and dielectric properties for Mg0· 6Cu0· 2Ni0· 2Cr2O4 chromite spinel, Phys. B Condens. Matter 624 (2022) 413439.
[65] M.Mubasher Mumtaz, Z. Saeed, Z. Sarfraz, Structural, dielectric, and impedance properties of MgFe2O4 nanoparticles and multi-walled carbon nanotubes nanocomposites, J. Supercond. Nov. Magnetism 35 (6) (2022) 1693–1702.
[66] C. Li, R. Xu, R. Gao, Z. Wang, G. Chen, X. Deng, W. Cai, C. Fu, Q. Li, Structure, dielectric, piezoelectric, antiferroelectric and magnetic properties of CoFe2O4–PbZr0. 52Ti0. 48O3 composite ceramics, Mater. Chem. Phys. 249 (2020) 123144.
[67] R. Gao, Q. Zhang, Z. Xu, Z. Wang, G. Chen, X. Deng, C. Fu, W. Cai, A comparative study on the structural, dielectric and multiferroic properties of Co0. 6Cu0. 3Zn0. 1Fe2O4/Ba0. 9Sr0. 1Zr0. 1Ti0. 9O3 composite ceramics, Compos. B Eng. 166 (2019) 204–212.
[68] N. Kumari, V. Kumar, S.K. Singh, Synthesis, structural and dielectric properties of Cr3+ substituted Fe3O4 nano-particles, Ceram. Int. 40 (8) (2014) 12199–12205.
[69] J.C.R. Araújo, S. Araujo-Barbosa, A.L.R. Souza, C.A.M. Iglesias, J. Xavier, P.B. Souza, C.C. Plá Cid, S. Azevedo, R.B. da Silva, M.A. Correa, S.N. de Medeiros, E. F. Silva, F. Bohn, Tuning structural, magnetic, electrical, and dielectric properties of MgFe2O4 synthesized by sol-gel followed by heat treatment, J. Phys. Chem. Solid. 154 (2021) 110051.
[70] A.R. Abraham, B. Raneesh, S. Joseph, P.M. Arif, P. Nambissan, D. Das, D. Rouxel, O.S. Oluwafemi, S. Thomas, N. Kalarikkal, Phys. Chem. Chem. Phys. 21 (2019) 8709–8720.
[71] M. Bitaraf, M.E. Ghazi, M. Izadifard, A study on structural, optical, and magnetic properties of MgFe2O4–BaTiO3 nanocomposites, J. Mater. Res. (2023) 1–13.
[72] T.F. Fuller, J.N. Harb, Electrochemical Engineering, John Wiley & Sons, 2018, 448.
[73] K. Agrawal, B. Behera, S.C. Sahoo, S.K. Rout, A. Kumar, D.K. Pradhan, P.R. Das, Dielectric, ferroelectric, magnetic and electrical properties of Sm-doped GaFeO3, Appl Phys A 128 (2) (2022) 1–17.
[74] M.V. Sokolova, V.V. Voevodin, J.I. Malakhov, N.L. Aleksandrov, E.M. Anokhin, V.R. Soloviev, Barrier properties influence on the surface dielectric barrier discharge driven by single voltage pulses of different duration, J. Phys. D Appl. Phys. 52 (32) (2019) 324001.
[75] M.D. Hossain, M.N.I. Khan, A. Nahar, M.A. Ali, M.A. Matin, S.M. Hoque, M.A. Hakim, A.T.M.K. Jamil, Tailoring the properties of Ni-Zn-Co ferrites by Gd3+ substitution, J. Magn. Magn Mater. 497 (2020) 165978.